Bažant, Z.P., and Pfeiffer, P. A. (1985)."Tests of shear fracture and strain-softening in concrete." Proc., *2nd Intern. Symposium on the Interaction of Non-nuclear Munitions with Structures.* held in Panama City Beach, Fla., pp. 254–264.

PROCEEDINGS
OF
SECOND SYMPOSIUM ON

THE INTERACTION OF NON-NUCLEAR MUNITIONS WITH STRUCTURES

PANAMA CITY BEACH, FLORIDA
APRIL 15-18, 1985

TESTS OF SHEAR FRACTURE AND STRAIN-SOFTENING IN CONCRETE

Zdeněk P. Bažant
and
Phillip A. Pfeiffer

Center for Concrete and Geomaterials
Northwestern University, Evanston, Illinois 60201

ABSTRACT

The paper reports fracture tests of double notched beam specimens of concrete and mortar loaded in shear. It is demonstrated that shear fracture propagation exists provided that there exists a concentrated shear zone. The results tend to confirm the maximum energy release rate criterion for fracture propagation. Tests of geometrically similar specimens yield maximum loads that agree with the recently established size effect law for blunt fracture, previously verified for Mode I. Preliminary results also indicate agreement with finite element analysis based on the strain-softening crack band model, in which the same material properties are assumed for fractures in Mode I and Mode II. The results are of particular interest for the failure of concrete structures subjected to blast loadings.

INTRODUCTION

Cracks in concrete or mortar have been generally assumed to propagate in the direction normal to the maximum principal stress, which represents the cleavage (or opening) fracture mode, designated as Mode I. This type of cracking has been verified even for the failure of many structures loaded in shear, e.g., the diagonal shear failure of beams, the punching shear failure of slabs, the torsional failure of beams, the shear failure of panels, etc. Ingraffea [1] showed recently that in a shear-loaded beam with a starter notch normal to the beam axis the crack does not propagate in this direction but roughly in the direction normal to the maximum principal stress. Thus, many investigators have thought that shear fracture does not exist, and even the claim that "shear fracture is a sheer nonsense" has been heard in some recent lectures.

Shear fractures are nevertheless observed in practice. For example, reinforced concrete slabs loaded by an intense short-pulse blast often fail by shearing off at the support along a crack normal to the slab. Penetration of projectiles into concrete also apparently involves shear-produced cracks. On the modeling side, applications of the recently developed crack band model with strain-softening [13,16,17,10] have indicated that the crack band which models fracture can propagate, under certain conditions, in the shear mode (Mode II).

Therefore, a program to investigate the shear fracture of concrete has been undertaken at Northwestern University, and presentation of the first results is the purpose of this paper.

TEST SPECIMENS

The test specimens were beams of constant rectangular cross section and constant length-to-depth ratio 8:3 (see Fig. 1). To determine the size effect, a crucial aspect of fracture mechanics, geometrically similar specimens of various depths, d = 1.5, 3, 6, and 12 in. (Fig. 2), were tested. The specimens of all sizes were cast from the same batch of concrete or mortar, and their thicknesses b were the same; b = 1.5 in.

For comparison of specimens of different sizes, the choice of their thicknesses is a subtle question which has no clear-cut answer. The question arises with respect to the effect of the probable variation of fracture energy along the crack edge across the thickness. This variation is principally due to two effects: 1) The fact that the crack front in the interior of the specimen is essentially in plane strain, while near the surface it is essentially in plane stress, which causes for elastic behavior an additional stress singularity at the surface termination of the crack edge [2]; and 2) The fact that nonplanar deformation at crack front near the surface may be caused by failures along planes nonorthogonal to the specimen sides, similarly to the shear-lip phenomenon in plastic fracture of metals [3,4,5]. The former effect would prevail for structures very large compared to the aggregate size, which would basically follow linear fracture mechanics. The latter effect seems to be more important for structures of normal sizes because the size of the fracture process zone affected by the surface would be proportional to the aggregate size and independent of the specimen size. Therefore, the latter effect was deemed to be more important, and this was the reason for choosing the same thickness for specimens of all sizes, ensuring the same thickness-to-aggregate size ratio.

A pair of symmetric notches, of depth $d/6$ and thickness 2.5 mm (same thickness for all specimen sizes) was cut with a diamond saw into the hardened specimens. (Compared to the specimen with a one-sided notch used before, the symmetrically notched specimen, in which two cracks propagate simultaneously, is simpler to analyze.) The specimens were cast with the side of depth d in a vertical posi-

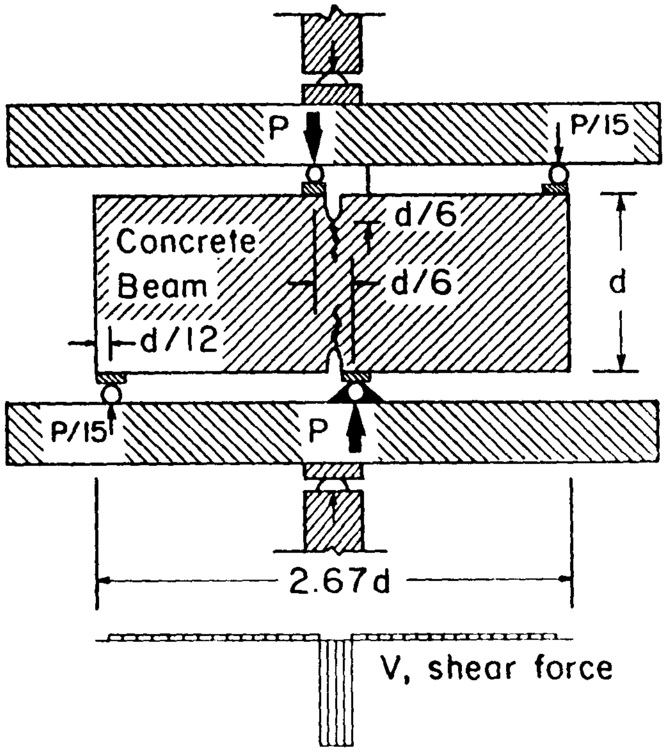

Fig. 1 - Mode II Fracture Specimen and Loading Apparatus.

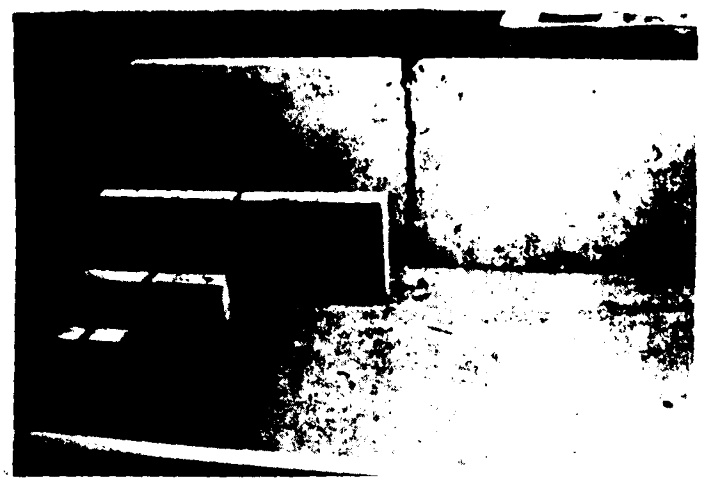

Fig. 2 - Specimens of Four Different Sizes, after Mode II Fracture

Fig. 3 - MTS Testing Machine with Specimen (after Test).

tion, using a concrete mix with water-cement ratio 0.6 and cement-sand-gravel ratio of 1:2:2 (all by weight). The maximum gravel size was $d_a = 0.5$ in., and the maximum sand grain size was 0.19 in. Mineralogically, the aggregate consisted of crushed limestone and siliceous river sand. The aggregate and sand were air-dried prior to mixing. Portland cement C150, ASTM Type I, with no admixtures, was used.

To illustrate the effect of aggregate size, a second series of specimens was made of mortar, with water-cement ratio of 0.5 and cement-sand ratio of 1:2. The same sand as for the concrete specimens was used, the gravel being omitted. Thus, the maximum aggregate size for the mortar specimens was $d_a = 0.19$ in. The water-cement ratio differed from that for concrete specimens in order to achieve approximately the same workability.

Companion cylinders 3 in. in diameter and 6 in. in length were cast from each batch of concrete or mortar to determine the compression strength. After standard 28-day moist curing, the compression strength was $f_c' = 5500$ psi with standard deviation S.D. = 125 psi for the concrete specimens, and 7100 psi with S.D. = 107 psi for the mortar specimens (each value determined from 3 cylinders).

The specimens were removed from the plywood forms after 1 day and were subsequently cured until the moment of the test, for 28 days, in a moist room of 95% relative humidity and 78F temperature. Three identical specimens were tested for each type of test.

The tests were carried out in a 10-ton servo-controlled closed-loop MTS testing machine (Fig. 3). The laboratory environment had relative humidity about 65% and temperature about 78F, and the specimens were exposed to this environment approximately 3 hours before the start of the test.

The shear loading was produced by a system of steel beams shown in Fig. 1, which applied concentrated vertical loads onto the specimen. Three of the loads were applied through rollers, and one through a hinge, which produced a statically determinate support arrangement. The steel surfaces were carefully machined so as to minimize the friction on the rollers.

The distribution of shear force V in the vertical cross sections, produced by this load arrangement, is shown in Fig. 1. Note that the loads were applied relatively close to the notches, so as to produce a narrow region of a high shear force. However, the loads could not be too close to the notch, or else the concrete under the support would shear off locally before the overall shear fracture could be produced. To prevent this from happening, the load-distributing steel plate under the roller could not be too small, and after some experimentation a suitable size of the support plate was determined. For the four specimen sizes, the support plates under the rollers and the hinge had the widths of 0.25, 0.5, 1 and 2 inches. The distance of the loads from the notch axis was always kept as d/12. The thickness of all loading plates was 0.25 in.

The specimens were tested at constant displacement rate of the machine. For each specimen size the displacement rate was selected so as to achieve the maximum load in about 5 min. (±30 sec.).

TEST RESULTS

The measured values of the maximum load measured are given in Table 1 for all specimens of all sizes, along with the mean values.

Table 1. - Measured Maximum Loads

Type of Test	Depth d (in.)	Maximum Load P, (lb.)			Mean $\bar{P}$
		1	2	3	
Mode II Concrete	1.5	1380	1465	1475	1440
	3.0	2792	2816	3012	2873
	6.0	5300	5580	5590	5490
	12.0	9910	9990	10100	10000
Mode II Mortar	1.5	1700	1735	1755	1730
	3.0	3200	3300	3350	3283
	6.0	5280	5400	5500	5410
	12.0	9200	9700	10000	9633
Mode I Concrete	1.5	405	408	417	410
	3.0	676	705	710	697
	6.0	984	1034	1090	1036
	12.0	1715	1716	1750	1727
Mode I Mortar	1.5	456	508	543	502
	3.0	702	751	776	743
	6.0	999	1053	1098	1050
	12.0	1461	1559	1565	1528

The cracks propagate as shown in Fig. 1. This proves that shear fracture exists, i.e., the crack can propagate in Mode II. Microscopically, of course, the shear fracture is likely to form as a zone of tensile microcracks with a predominantly 45°-inclination which only later connect by shearing; but the fact is that in the macroscopic sense the observed fractures must be described as Mode II.

As already mentioned, the presently observed crack direction contrasts with that observed by Ingraffea [1] in his test sketched in Fig. 4a. This test differed by its wider separation of the loading points. Therefore, the present type of test was also made with a wider separation of the loading points. In that case the cracks propagated from the notch tip basically in the direction normal to the maximum principal stress, same as observed by Ingraffea; see Fig. 4b. In both the present type of test (Fig. 1) and the tests with the wide shear zone (Fig. 4a,b) the stress fields near the fracture front are similar. So the crack somehow senses the stress field remote from the cracks, and responds to it. Consequently, the stress field near the fracture front, as well as the strain and strain energy density fields near the fracture front, does not govern the direction of fracture propagation. What is then the governing law?

The answer is that a Mode I crack propagating sideway from the notch tip would, for the present type of test with a narrow shear force zone, quickly run into a low stress zone of the material, and would, therefore, release little energy. On the other hand, a vertically running crack (Mode II) continues to remain in the highly stressed zone of

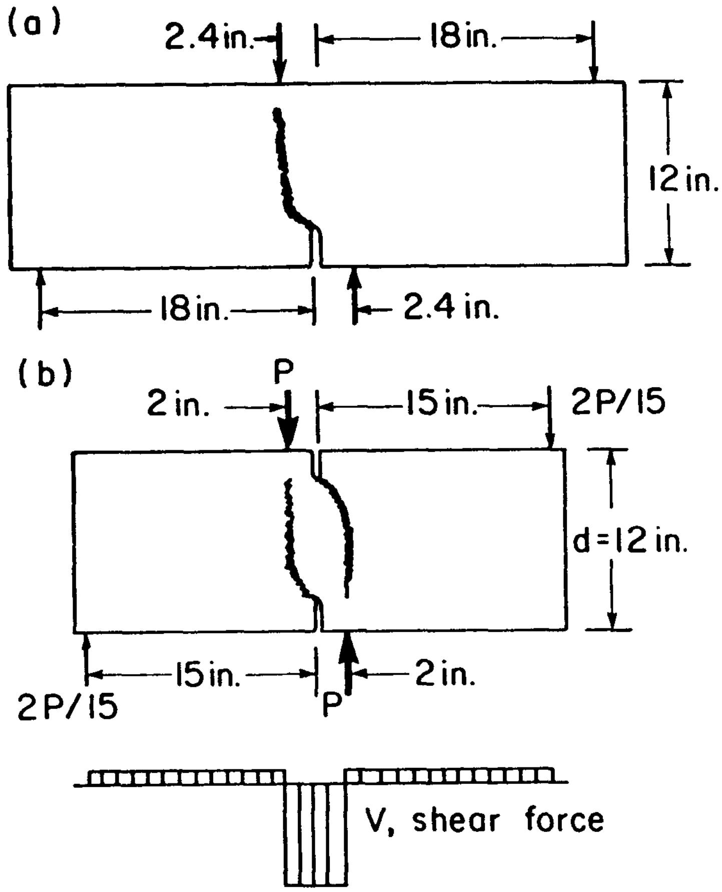

Fig. 4 - Crack Paths Obtained when Shear Zone is not Concentrated.

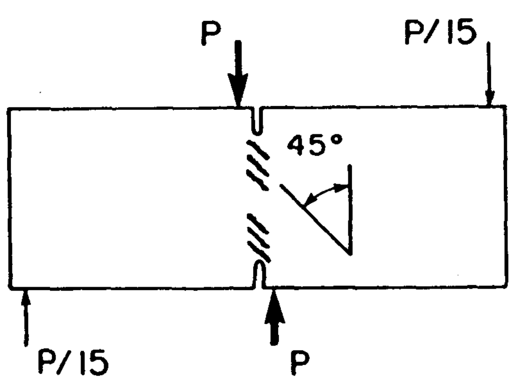

Fig. 5 - Mode II Fracture Arising from a Band of Mode I Microcracks.

the material, and can, therefore, cause a large release of strain energy. This appears to confirm that the fracture propagation direction is governed by the criterion of the maximum energy release rate. This criterion has been known in theoretical fracture mechanics and is in fact a direct consequence of the basic laws of thermodynamics.

The conclusion that the criterion of maximum energy release rate should govern the direction of crack propagation is confirmed by the finite element studies reported by Pfeiffer et al. [6-9]. In these studies, the crack band model was used, and among all finite elements adjacent to the crack band front the crack band was advanced into that element for which the energy release from the finite element system was maximum. These finite element simulations indicated the crack band to propagate sideway when the shear force zone was wide (Fig. 4b), and vertically when the shear force zone was narrow (Fig. 1), which is in agreement with the observed directions of crack propagation.

SIZE EFFECT AND FRACTURE ENERGY

The structural size effect, a salient aspect of fracture mechanics, is observed when geometrically similar structures of different characteristic dimensions d are compared. It can be described in terms of the nominal stress at failure, defined as $\sigma_N = P/bd$ where P = load at failure (maximum load) and b = structure thickness. While according to the strength or yield criteria used in plastic limit design or elastic allowable stress design, σ_N is independent of structure size d, in fracture mechanics σ_N decreases as the structure size increases. This is because fracture mechanics is based on energy criteria for failure.

Introducing an approximate but apparently quite reasonable hypothesis that the energy release caused by fracture is a function of both the fracture length and the area traversed by the fracture process zone, Bažant showed [10,11] by dimensional analysis and similitude arguments that, for geometrically similar structures of specimens,

$$\sigma_N = Bf_t'\left(1 + \frac{d}{\gamma_0 d_a}\right)^{-1/2} \quad (1)$$

in which f_t' is the direct tensile strength of concrete, d_a is the maximum aggregate size, and d, γ_0 are empirical parameters characterizing the shape of the structure or specimen. According to this size effect law, the plot of $\log \sigma_N$ vs. $\log (d/d_a)$ represents a gradual transition from the strength criterion (i.e., σ_N proportional to strength f_t') to the failure criterion of the classical, linear elastic fracture mechanics (i.e., σ_N proportional to $d^{-1/2}$). This size effect law is verified, within the limits of inevitable statistical scatter, by all available Mode I fracture tests of concrete and mortar. Moreover, this size effect law has also been shown applicable to the diagonal shear failure of longitudinally reinforced beams without stirrups [12], and is probably applicable to all the so-called brittle failures of reinforced concrete structures. Does the size effect law also apply to shear fracture?

The measured maximum load values show that it does. They are plotted in Fig. 6 as the data points, while the size effect law is plotted as the smooth curve, and a good agreement is apparent. Parameters B and γ_0 of the size effect law can be most easily obtained by the linear regression plot in Fig. 6 because Eq. 1 can be rearranged as $Y = AX + C$ where $X = d/d_a$, $Y = (f_t'/\sigma_N)^2$, $C = 1/B^2$, $A = 1/(\gamma_0 B^2)$. This means that $B = 1/\sqrt{C}$, $\gamma_0 = 1/(AB^2)$ where A represents the slope of the straight regression line in Fig. 6 and C represents its intercept with axis Y.

An advantage of the regression plot is that it also yields statistics of the errors, i.e., of the deviations of the measured data points from the size effect law. As is clear from Fig. 6, these deviations are random rather than systematic, and their coefficient of variation is found to be $\omega_{Y|X} = 0.0911$, which is quite acceptable for a heterogeneous material with statistical properties such as concrete. This value is calculated as $\omega_{Y|X} = \{[\Sigma(Y - Y_{test})^2]/(N-2)\}^{1/2}/\bar{Y}$, which is an unbiased estimate; $Y - Y_{test}$ are the deviations of data points, N is the number of all data points, and $\bar{Y} = (\Sigma Y)/N$ = mean of all measured Y. When the statistics is based on the mean P for each specimen size, then $\omega_{Y|X} = 0.0668$.

To calibrate the size effect law once its validity is already accepted requires specimens whose sizes differ at least as 1:3. However, to verify the validity of the size effect law one needs a much broader range of sizes, at least 1:10. This necessitates inclusion of very large specimens in the test program. The smallest specimen is chosen as small as possible for the given size of aggregate. This is the reason for choosing the depth of the smallest specimen to be only $3d_a$. The largest practicable specimen for the available testing machine was then of depth d = 12 in. (d/d_a = 24). For concrete, however, this size is not large enough to verify the size effect law (Eq. 1), since the last data points for concrete in Fig. 6 lie too far from the limiting inclined straight line of slope - 1/2 corresponding to linear elastic fracture mechanics. This was the main reason for adding a second series of mortar specimens, which makes it possible to extend substantially the range of relative sizes d/d_a without having to test still much larger specimens. Even though some additional error is no doubt introduced due to the differences between mortar and concrete other than those due to aggregate size d_a, the measured maximum loads for concrete and mortar, when put together, appear to follow quite well the size effect law (Eq. 1), and thus to verify its validity.

Note also that according to Fig. 6 linear fracture mechanics would govern the behavior of specimens with d/d_a = 200 or larger. This implies for concrete the beam depth of over 100 in., and for mortar over 40 in.

Another advantage of the size effect law is that it allows the simplest way to determine the fracture energy G_f. As recently shown [14],

$$G_f = \frac{g(\alpha_0)}{A\,E_c}(f_t')^2 d_a \quad (2)$$

in which A = slope of the size effect regression

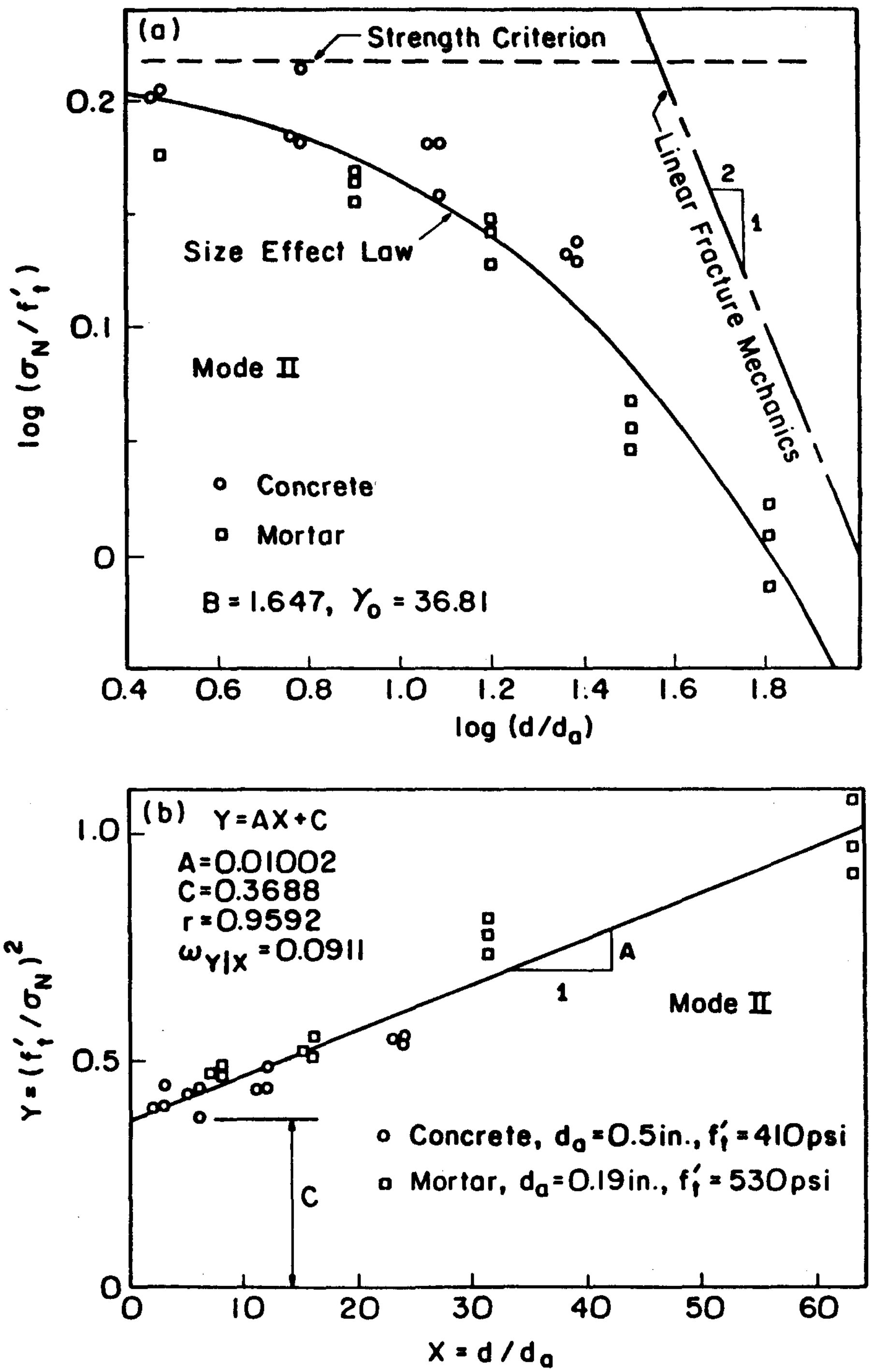

Fig. 6 - Test Results of Mode II (shear) Fracture Tests and their Regression.

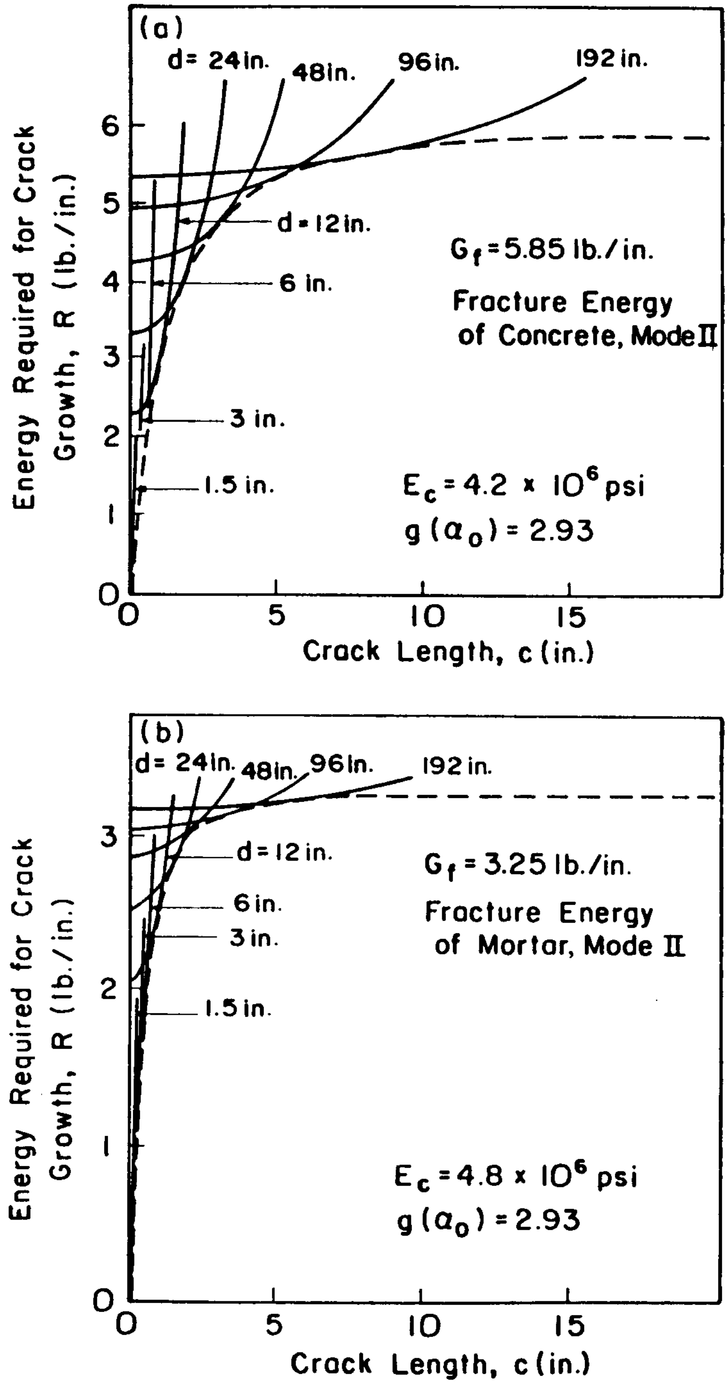

Fig. 7 - R-Curves Derived from Mode II Fracture Test Results

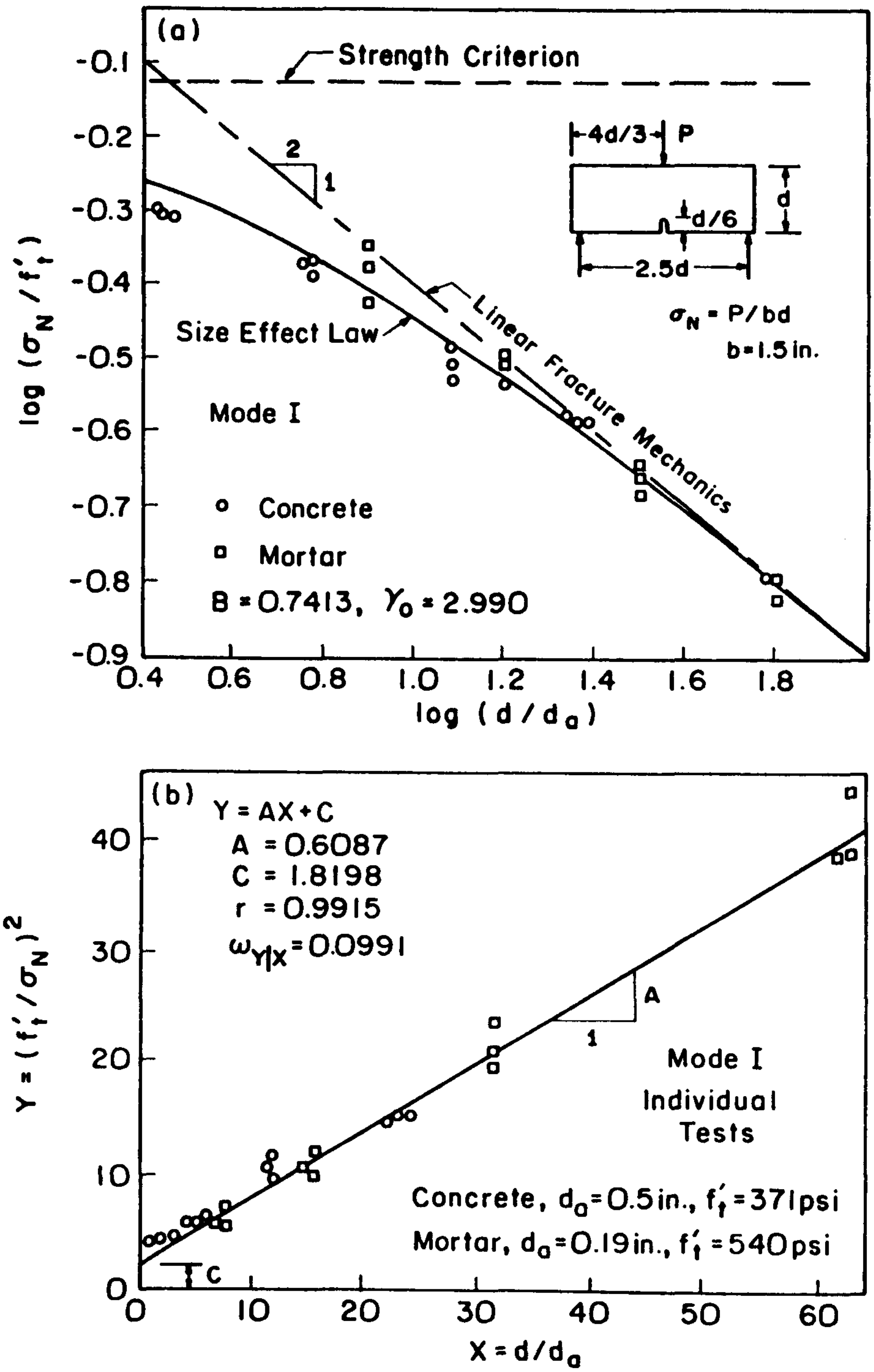

Fig. 8 - Test Results of Mode I Fracture Tests and Their Regression.

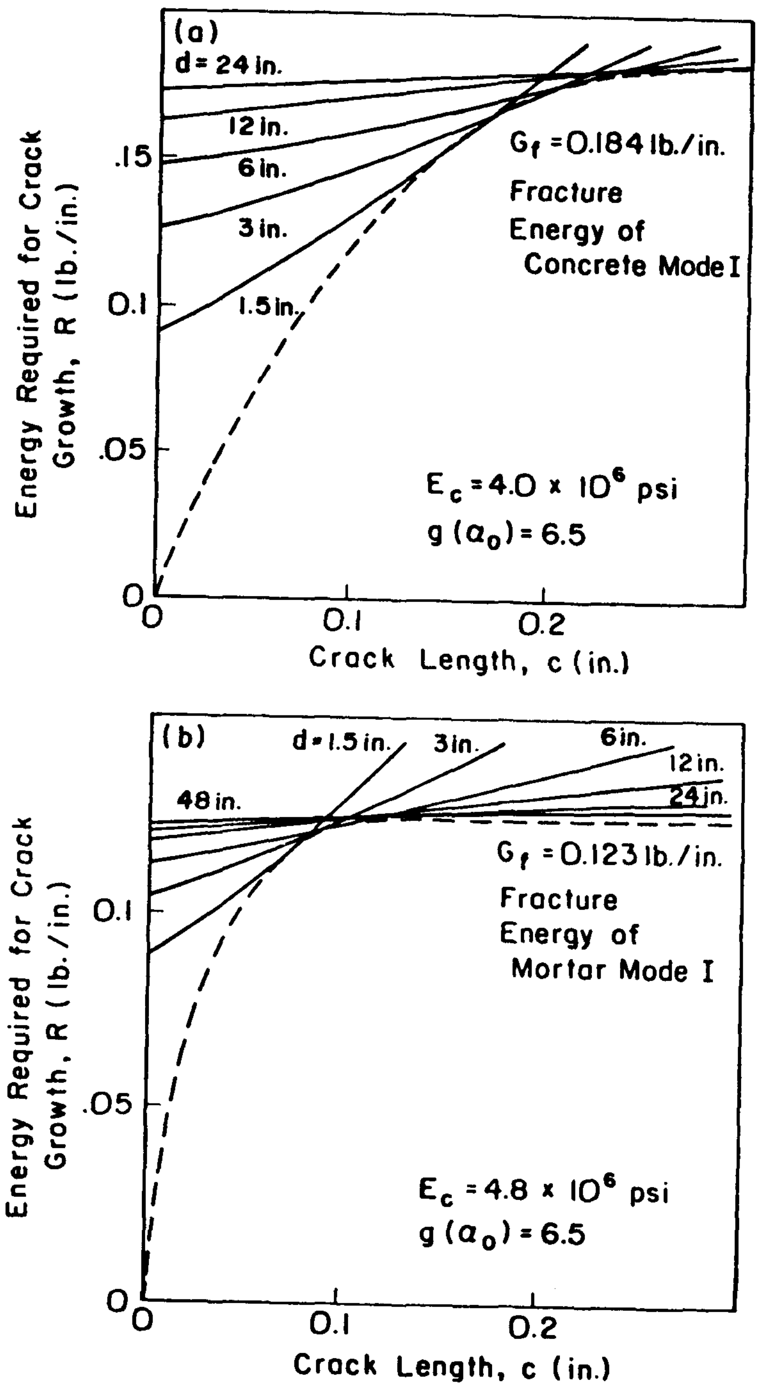

Fig. 9 - R-Curves Derived from Mode I Fracture Test Results.

line (Fig. 7b in the present case), E_c = elastic Young's modulus, and $g(\alpha_0) = G(\alpha_0)E_c b^2 d/P^2$; $G(\alpha)$ represents the linearly elastic energy release rate as a function of $\alpha = a/d$ where $a = a_0 + c$, a_0 = length of the notch and c = length of the crack from the notch tip, $G(\alpha_0)$ is the value of G evaluated for $a = a_0$, and $g(\alpha_0)$ with $\alpha_0 = a_0/d$ is the nondimensional energy release rate. The values of $G(\alpha_0)$ or $g(\alpha_0)$ can be found in handbooks [15] or textbooks [3,4,5] for many typical specimen geometries, however, not for the present specimen. Therefore, the value of $g(\alpha_0)$ was obtained by linear elastic finite element analysis; $g(\alpha_0) = 2.93$.

Note that f_t' and d_a are used in Eq. 2 because the regression plot in Figs. 6 and 7 is in nondimensional variables in order to allow comparing mortar and concrete. Alternately, the regression could be done in the plot of σ_N^{-2} versus d, and then $f_t'^2$ and d_a do not appear in Eq. 2. Therefore, the precise values of f_t' (and d_a) are immaterial for the value of G_f calculated in Eq. 2.

Application of Eq. 2 to the present data yields the following values for Mode II fracture energy $G_f = G_f^{II}$;

$$G_f^{II} = 5.85 \text{ lb./in. (1020 N/m) for concrete}$$
$$G_f^{II} = 3.25 \text{ lb./in. (539 N/m) for mortar.} \qquad (3)$$

From preliminary results of the companion Mode I test series for the same type of concrete and mortar, application of Eq. 2 (for the three-point bent specimen geometry) yields approximately the value G_f^I = 0.184 lb./in. (32.2 N/m) for concrete and G_f^I = 0.123 lb./in. (21.5 N/m) for mortar. The linear regression plot and size effect are plotted in Fig. 8 for individual maximum load values. The load values for Mode I fracture tests are given in Table 1.

It is striking how much larger the fracture energy is for Mode II as compared to Mode I. The ratio appears to be about 32 for concrete and 26 for mortar. This huge difference seems, however, explicable in terms of the crack band finite element model [16] which was shown to also describe correctly the crack shear resistance [17].

The results of tests and of preliminary finite element calculations compare as follows:

$$\text{Tests:} \quad G_f^I = 0.184 \text{ lb./in.}, \; G_f^{II} = 5.85 \text{ lb./in.}$$
$$\text{Finite Elements:} \quad G_f^I = 0.236 \text{ lb./in.}, \; G_f^{II} = 5.02 \text{ lb./in.} \qquad (4)$$

It must be emphasized that the same material properties, defined by the same tensile strain-softening diagram [16], were used both for Mode I and Mode II finite element simulations.

In Mode I fracture, the fracture energy is in the crack band model represented by the area under the tensile strain-softening diagram, multiplied by the width of the fracture process zone. In Mode II (shear) fracture, tensile cracking is not all that is needed for failure. The cracks produced by shear are inclined about 45°, and there remains a connection across the fracture after these cracks form, consisting of inclined struts between the cracks spanning across the fracture (Fig. 6).

The full shearing of the material also requires that these struts be broken by compression crushing (which would most likely consist in compression-shear failure of these struts). Therefore, the fracture energy for shear also includes the area under the compression stress-strain diagram for these inclined struts, including the strain-softening portion of this diagram, multiplied by the width of the fracture process zone. Now, the area under the complete compression stress-strain diagram is many times larger than the area under the complete tensile stress-strain diagram. Thus, it is not surprising that the G_f-values in Eq. 3 are far larger than those for Mode I fracture. It must be kept in mind, however, that these values of G_f^{II} include the energy to break the shear resistance due to aggregate interlock (crack surface roughness).

The size effect law also makes it possible to easily determine the R-curve, i.e., the plot of the energy required for crack growth as a function of the crack length, c (measured from the notch tip). As shown in Refs. 14 and 19, the R-curve represents the envelope of the fracture equilibrium curves of geometrically similar specimens of all sizes; see Figs. 7, 8 and 9, in which the convex curve for each specimen depth d can be plotted from the maximum load value, P [14,19]. It is essential to use for this purpose the maximum load values smoothed by the size effect law. If the use of unsmoothed, scattered data (as measured) is attempted, then the fracture equilibrium curves do not yield any envelope [14,19]. As already remarked, the limiting asymptotic value of the envelope, i.e., of the R-curve, is the fracture energy obtained from Eq. 2. Fig. 7 shows the R-curve for shear fracture obtained after smoothing with the regression line in Fig. 6. (Fig. 9 shows the R-curve for Mode I fracture from regression line in Fig. 9.) Availability of the R-curve makes it possible to approximately calculate failure loads of structures with an equivalent analysis based on linear elastic fracture mechanics, even though the fracture law is evidently highly nonlinear.

A more detailed study of the finite element modeling of shear fracture with the crack band model is planned for subsequent work. While the crack band model and the finite element models based on a stress-displacement relation for a line crack (Hillerborg's model, Refs. 18 and 19) are essentially equivalent for Mode I fracture tests of concrete and can represent them equally well, there appears to be a significant difference for shear fracture tests. It seems that both Mode I and Mode II fracture tests can be described with one and the same crack band model. This is not true for the model based on the stress-displacement relation, for which some additional rules apparently need to be added to make it work also for shear fracture and, in particular, to represent the contribution of surface roughness (aggregate interlock) to the shear fracture energy.

CONCLUSIONS

1. Shear fracture (i.e., Mode II fracture) of concrete exists.
2. The direction normal to the maximum principal stress cannot be considered in general as a

criterion of crack propagation direction in concrete. Rather, fracture seems to propagate in the direction for which the energy release rate from the fracture is maximized.

3. Like Mode I fracture, the shear (Mode II) fracture follows the size effect law of blunt fracture [11]. This implies that a large fracture process zone must exist at the fracture front, and that nonlinear fracture mechanics should be used, except for extremely large structures.

4. The maximum aggregate size d_a appears acceptable as a characteristic length for the size effect law. This further implies that the size of the fracture process zone at maximum load is approximately a certain fixed multiple of the maximum aggregate size.

5. The shear (Mode II) fracture energy appears to be about 32-times larger than the cleavage (Mode I) fracture energy. This large difference may probably be explained by the fact that shear fracture energy includes not only the energy to create inclined tensile microcracks in the fracture process zone, but also the energy required to break the shear resistance due to interlock of aggregate and other asperities on rough crack surfaces behind the crack front.

6. The R-curve describing the shear fracture energy required for crack growth as a function of the crack extension from the notch, may be obtained from the size effect law. It results as the envelope of the fracture equilibrium curves for geometrically similar specimens of various sizes.

ACKNOWLEDGMENT

Partial financial support under U.S. Air Force Office of Scientific Research Grant No. 83-0009 to Northwestern University, monitored by L. Hokanson, is gratefully acknowledged.

REFERENCES

1. Arrea, M., and Ingraffea, A. R., "Mixed-mode Crack Propagation in Mortar and Concrete," Dept. of Structural Engineering, Cornell University, Report No. 81-13, 1982.
2. Bažant, Z. P., and Estenssoro, L. F., "Surface Singularity and Crack Propagation," *Int. J. of Solids and Structures, 15,* 1979, pp. 405-426, Addendum, *16*, pp. 479-481, Errata, *19*, p. 661.
3. Broek, D., *Elementary Engineering Fracture Mechanics*, Sijthoff and Noordnoff, Alphen aan den Rijh, Netherlands, 1978.
4. Knott, J. F., *Fundamentals of Fracture Mechanics,* Butterworths, London, England, 1973.
5. Rolfe, S. T., and Barsom, J. M., *Fracture and Fatigue Control in Structures,* Prentice-Hall, Englewood Cliffs, N.J., 1977.
6. Pfeiffer, P. A., "Blunt Crack Band Propagation in Finite Element Analysis for Concrete Structures," Argonne National Laboratory, RAS 83-10, March 1983.
7. Pfeiffer, P. A., Marchertas, A. H., and Bažant, Z. P., "Blunt Crack Band Propagation in Finite Element Analysis for Concrete Structures," *Transactions of 7th International Conference on Structural Mechanics in Reactor Technology,* Paper H5/2, North-Holland, Amsterdam, 1983, pp. 227-234.
8. Pan, Y. C., Marchertas, A. H., and Kennedy, J. M., "Finite Element of Blunt Crack Propagation, A Modified J-integral Approach," *Transactions of 7th International Conference on Structural Mechanics in Reactor Technology,* Paper H5/3, North-Holland, Amsterdam, 1983, pp. 235-292.
9. Pan, Y. C. Marchertas, A. H., Pfeiffer, P. A., and Kennedy, J. M., "Concrete Cracking Simulations for Nuclear Applications," *Theoretical and Applied Fracture Mechanics, 2,* No. 1, 1984, pp. 27-38.
10. Bažant, Z. P., "Fracture in Concrete and Reinforced Concrete," Preprints, IUTAM Prager Symposium on *Mechanics of Geomaterials: Rocks, Concretes, Soils,* ed. by Z. P. Bažant, Northwestern University, Sept. 1983, pp. 281-316.
11. Bažant, Z. P., "Size Effect in Blunt Fracture: Concrete, Rock, Metals," *Journal of Engineering Mechanics, ASCE, 110,* No. 4, 1984, pp. 518-535.
12. Bažant, Z. P., and Kim, J. K., "Size Effect in Shear Failure of Longitudinally Reinforced Beams," *Journal of the American Concrete Institute, 81,* No. 5, Sept.-Oct. 1984, pp. 456-468.
13. Bazant, Z. P., "Crack Band Model for Fracture of Geomaterials," Proc. 4th Intern. Conf. on Numer. Methods in Geomechanics," ed. by Z. Eisenstein, held in Edmonton, Alberta, 1982, Vol. 3, pp. 1137-1152.
14. Bažant, Z. P., Kim, J. K., and Pfeiffer, P., "Determination of Nonlinear Fracture Parameters from Size Effect Tests," NATO Advanced Research Workshop on *Application of Fracture Mechanics to Cementitious Composites,* ed. by S. P. Shah, Northwestern University, Sept. 4-7, 1984, pp. 143-169.
15. Tada, H., Paris, P. C., and Irwin, G. R., *The Stress Analysis of Cracks Handbook,* Del Research Corp., Hellertown, Pa., 1973.
16. Bažant, Z. P., and Oh, B. H., "Crack Band Theory for Fracture of Concrete," *Materials and Structures* (RILEM, Paris), *16*, 1983, pp. 155-177.
17. Bažant, Z. P., and Gambarova, P. G., "Crack Shear in Concrete: Crack Band Microplane Model," *Journal of Structural Engineering. ASCE, 110,* No. ST9, Sept. 1984, pp. 2015-2035.
18. Hillerborg, A., Modéer, M., and Petersson, P. E., "Analysis of Crack Formation and Crack Growth in Concrete by Means of Fracture Mechanics and Finite Elements," *Cement and Concrete Research, 6,* 1976, pp. 773-782.
19. Petersson, P. E., "Crack Growth and Development of Fracture Zones in Plain Concrete and Similar Materials," thesis presented to the Lund Institute of Technology, at Lund, Sweden, in 1981, in partial fulfillment of the requirements for the degree of Doctor of Philosophy.